Mon. Not. R. Astron. Soc. **000**, 000–000 (0000) Printed 19 July 2013 (MN LATEX style file v2.2)

The backbones of stellar structures in barred-spiral models -the concerted action of various dynamical mechanisms on galactic discs

L. Tsigaridi,[1,2⋆] P.A. Patsis[1]
[1]*Research Center for Astronomy, Academy of Athens, Soranou Efessiou 4, GR-115 27, Athens, Greece*
[2] *Section of Astrophysics, Astronomy and Mechanics, Department of Physics, University of Athens, Greece*

Accepted .....Received .....;in original form .....

ABSTRACT
We investigate the dynamics of a barred-spiral model, rotating with a single pattern speed, which is characterized by a corotation-to-bar-radius ratio (R_c/R_b) about 2.9. The response morphology of the model consists of an inner barred-spiral structure, surrounded by an oval-shaped disc and a fainter set of arms at larger radii. The oval-shaped disc and the barred-spiral structure included in it are located inside corotation, while the outer spiral arms extend beyond it. The system harbours two main different dynamical mechanisms, which shape its morphology. The bar and the spiral arms inside corotation are structured to a large extent by regular orbits, while the spiral arms beyond corotation are built by chaotic orbits. Chaotic orbits play a role also inside corotation, specifically in building weak extensions of the inner spirals as well as in the central part of the bar. The oval-shaped disc is also shaped by chaotic orbits. For the outer spirals, we find that the vast majority of the chaotic orbits, which reinforce the spirals at least for a time interval of 8 pattern rotations, includes in its morphology the imprints of "4:1-resonance-like" orbits, in agreement with previous studies, as well as of "long-period-banana-like" orbits. Both of them belong to orbits of the *"hot orbital population"* that visit both areas, inside and outside corotation. This orbital population plays the key role for supporting structures out of chaos. In the case we study order and chaos cooperate in building a galactic morphology that is encountered among grand design spiral galaxies (NGC 1566 and NGC 5248). The fact that in the model are implicated, on one hand the "precessing ellipses flow" supporting the spiral arms of normal spirals and on the other hand the "chaotic spirals" found in barred-spiral systems, indicates that it is a model bridging two different orbital stellar dynamics.

Key words: Galaxies: kinematics and dynamics – Galaxies: spiral – Galaxies: structure

1 INTRODUCTION

This paper revisits the orbital dynamics of barred-spiral systems. We investigate all possible dynamical mechanisms that shape a barred-spiral morphology. The question we address is about the types of orbits that participate in building the spiral arms and the bar. Is there a unique solution to this problem and if not, under which conditions is one or the other mechanism activated? The understanding of this procedure has major implications on the overall dynamics of the discs, since the character of the orbits that support the spiral arms and the bar is directly related with the location of corotation, in other words with the pattern speed of the system. Furthermore, different structure-supporting mechanisms point towards different stellar flows in the discs and this difference affects in turn also the gaseous flows and subsequently the star formation procedures.

⋆ liana@academyofathens.gr (LT); patsis@academyofathens.gr (PAP)

In non-barred spirals, *regular, quasi-periodic* orbits provide support to the spiral arms up to the inner 4:1 resonance (Contopoulos & Grosbøl 1986, 1988; Patsis et al. 1991; Martos et al. 2004; Lépine et al. 2011), provided that the gravitational potential does not change considerably at least over several pattern periods.

In barred-spiral models on the other hand it has been proposed that the particles on the arms follow both *chaotic and regular* orbits (Kaufmann & Contopoulos 1996), or only chaotic orbits (Voglis & Stavropoulos 2005; Patsis 2006; Voglis et al. 2006; Romero-Gómez et al. 2006). This latter idea has been developed and elaborated mainly by two groups in long series of papers. The interested reader may refer to recent extended, or review articles (Contopoulos 2009; Athanassoula et al. 2010; Efthymiopoulos 2010; Patsis 2012) and references therein. The basic idea is that particles following the unstable branch of the manifolds associated with the families of unstable periodic orbits surrounding the unstable Lagrangian points L_1 and L_2 close to the ends of the bar (called PL1

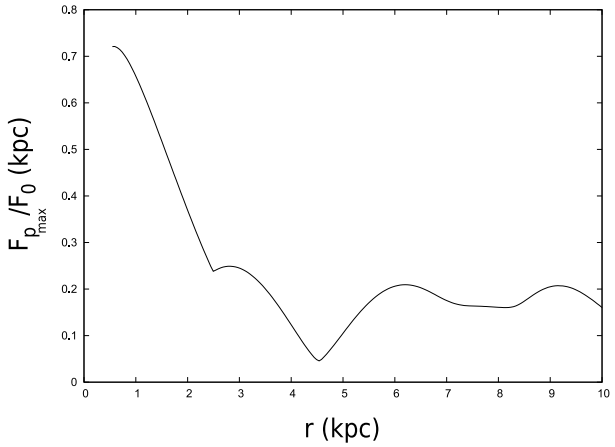

Figure 1. The radial variation of the maximum force of the perturbation $F_{p_{max}}$, with respect to the axisymmetric force, F_0, in our main model.

and PL2 families by Tsoutsis et al. (2009)), form the spiral arms, which extend beyond the corotation of the system.

Chaotic orbits of particles participating in the formation of spiral arms have been studied also in *N*-body models (Voglis et al. 2006; Tsoutsis et al. 2008; Harsoula & Kalapotharakos 2009; Harsoula et al. 2011; Athanassoula 2012). These orbits reflect the orbital behaviour of the "hot orbital population" discussed initially by Pfenniger & Friedli (1991).

Nevertheless, results from other studies indicate that the mechanism based on the chaotic orbits in the neighbourhood of PL1 and PL2 cannot be considered as unique for explaining all observed barred-spiral morphologies of disc galaxies. Patsis et al. (2009) have presented a response model for the SB(rs)c type galaxy NGC 3359 (de Vaucouleurs et al. 1991, RC3), which matches the structure of the spiral arms only if the particles on the spirals follow a "precessing-ellipses flow", i.e. their orbits are regular (quasi-periodic). In such a case, if one wants to have a bar ending close to its corotation the bar should have a pattern speed different from the pattern speed of the spirals. The same potential for faster pattern speeds developed "chaotic spirals" (as we will call hereafter the spirals supported by particles in chaotic motion). However, these spiral arms were totally out of phase with respect to the spiral arms of the modelled galaxy.

As regards the *chaotic orbits* some works emphasize specific features, which are associated with the particular energy ranges, over which these orbits exist. One can even find particular structure-supporting mechanisms decoupled from the presence of PL1 and PL2. Specifically, (a) Patsis (2006) and Patsis et al. (2010) underline the fact that the orbits they find to support the spirals in potentials estimated from near-infrared observations have a strongly 4:1 resonance morphological character, (b) Tsoutsis et al. (2008) show that the unstable manifolds of *all* the families of unstable periodic orbits near and beyond corotation contribute to the support of the spiral structure and (c) Patsis et al. (2010) describe a mechanism for reinforcing spiral arms by chaotic orbits *inside* corotation.

On top of this, chaos seems to be responsible also for part of the structure of the bars themselves in many cases. Already Kaufmann & Contopoulos (1996) presented orbits contributing to the surface density of the bars and the spirals. Patsis et al. (1997) explained the outer envelope of the bar of NGC 4314 by means of chaotic orbits at the 4:1 resonance region. Patsis (2005) presented chaotic orbits supporting a ring morphology in 2D Ferrers bars and concluded that in some cases in order to understand the orbital behaviour of barred galaxies we have to look for structures supported by chaotic orbits. Chaotic envelopes of bars have been also found in the *N*-body models by Voglis et al. (2006). They are built by orbits of the same character as those building the chaotic envelopes of the bar of the NGC 4314 model in Patsis et al. (1997) and Patsis (2006). They are typical orbits of the "hot orbital population" (Pfenniger & Friedli 1991).

Furthermore in the potential for NGC 1300, estimated by Kalapotharakos et al. (2010) and studied by Patsis et al. (2010), the change of the pattern speed resulted to such a deformation of the effective potential isocontours in the bar region in a certain range of pattern speed values, so that their shape was of an ansae morphology. In this case we had multiple Lagrangian points roughly along the major axis of the bar. In general bars are supported by the x1 family of orbits (Contopoulos & Grosbøl 1989). However, in the models by Patsis et al. (2010), an ansae type bar in the response surface density could be sustained mainly by chaotic orbits instead of the typical x1 family of stable periodic orbits. The fact that the set of parameters characterizing these models is typical for barred-spiral galaxies, poses the question about how common could such "chaotic bars" be.

An alternative approach for the dynamics of spirals has been proposed by Zhang & Buta (2007). In this approach collective dissipation effects play a key role. This leads in many cases to different corotation radii than those suggested for the corresponding galactic types in the papers mentioned thus far in the introduction. In the Zhang & Buta (2007) models a different orbital content is expected, so that foreseen extensions of the bars beyond corotation and other features could be justified.

In general, the dynamics of a bar, or of a barred-spiral system, cannot be inferred just by inspection of its morphology. Qualitatively similar looking barred-spiral morphologies may appear in snapshots of N-body simulations during time intervals in which the bar rotates either fast or slowly (cf. the morphologies in the models by Athanassoula & Misiriotis (2002) and in the recent simulations by Saha & Naab (2013), as well as the barred-spiral morphologies appearing during the evolution of these models).

The aims of the present paper are:

- To find all possible dynamical mechanisms that could support the spiral arms in barred-spiral systems.
- To understand the conditions under which each mechanism appears.

The barred-spiral perturbations we study in our paper are strong. Our approach to the problem is based on orbital theory. Non-linear effects dominate and as a result the morphologies we study in our models are established within a few dynamical times. The longevity of these structures or the possible successive activation of the mechanisms we describe in the present paper during the evolution of a disc galaxy over a Hubble time, should be studied by means of *N*-body models.

The structure of the paper is the following: In Section 2 we describe the model we use in our calculations and in Section 3 we outline the method we followed in our study. The results are presented in 4, where we divide the model in four regions and we describe the dynamical mechanisms acting in each one of them in Sections 4.2 to 4.6, giving special attention to the role of the "hot orbital population" of orbits, described in 4.4. Finally we discuss our results and enumerate our conclusions in Section 5.

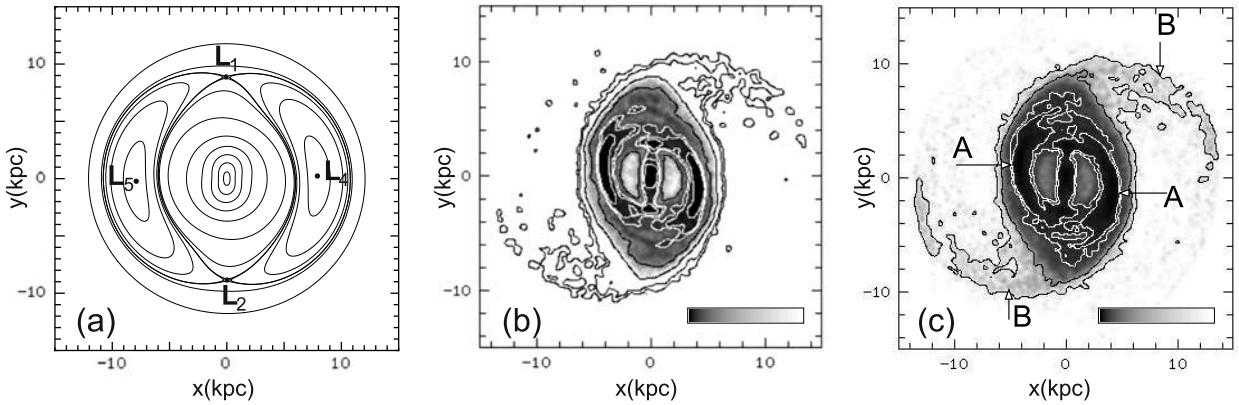

Figure 2. (a) Isocontours of the effective potential. We indicate the location of the stable Lagrangian points L_4 and L_5 as well as that of the unstable points L_1 and L_2. (b) The stellar response of the model after 10 bar rotations starting from circular velocities in the axisymmetric background. (c) The same as in (b) in a model with initial conditions with a certain dispersion of velocities (see text). The grey scale bars embedded in the frame gives the density scale. Darker shades correspond to denser regions. "A" and "B" point to the inner and the outer spirals respectively.

2 THE MODEL

Our potential in the plane of the galaxy is expressed in the form of a Fourier series so that

$$\Phi(r,\varphi) = \Phi_0(r) + \sum_{m=2,4,6} \Phi_{mc}(r)\cos(m\varphi) + \Phi_{ms}(r)\sin(m\varphi) \quad (1)$$

The components $\Phi_0(r)$, $\Phi_{mc}(r)$, and $\Phi_{ms}(r)$ of the equation above are given as polynomials of the form $\sum_n a_n r^n$, $n = 0 \ldots 8$.

We have taken as basis the NGC 3359 potential as estimated by Patsis et al. (2009) from near-infrared observations under some assumptions for the thickness of the disc, the M/L ratio and the distribution of dark matter. Despite the fact that observed morphologies even in the near infrared may deviate from the actual mass distribution (Zibetti et al. 2009) the model we use here is quite realistic. The near infrared observations of a real galaxy are taken as a basis for obtaining a well behaved barred-spiral potential. By changing properly the a_n values of the coefficients, we increased the strength of the bar and we decreased the strength of the higher order terms (m=2,4,6) so that we have a maximum force perturbation as described in Fig. 1. The plotted curve gives the ratio of the maximum non-axisymmetric perturbing force at a given radius $[(\partial\Phi_p/\partial r)^2 + (r^{-1}\partial\Phi_p/\partial\varphi)^2]^{1/2}$ to the total axisymmetric force $|d\Phi_0/dr|$, where Φ_p and Φ_0 are the potential of the non-axisymmetric and axisymmetric terms respectively. In this way we study a barred-spiral potential which has the following advantages:

(i) It has a dominating m=2 term and it is expected to follow archetypal dynamics for a wide range of late types barred-spiral morphologies in the Hubble sequence.

(ii) It is realistic because it originates from the NGC 3359 potential, which is a galaxy with a well defined barred-spiral structure.

(iii) It has an explicit self-gravitating spiral arm component.

(iv) It has a smooth transition at the end of the bar and beginning of spirals' region.

However, the adoption of a gravitational field originating from a potential estimation of a real galaxy has always a known disadvantage, namely that we know it up to a certain distance from the centre of the galaxy. This makes such potentials less appropriate for studies of orbits which visit large distances from the centre of the system and eventually escape. In our models we trust our potential up to a radius $r \approx 12.5$ kpc.

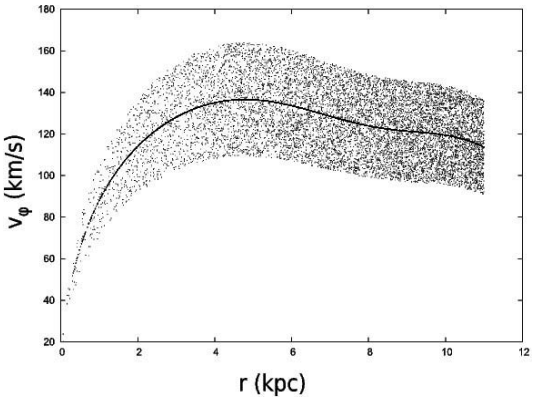

Figure 3. The initial tangential velocities in the case of the response model in Fig. 2c.

Our calculations are performed in a frame rotating with *a single pattern speed*. We try to understand the dynamics as the pattern speed of the barred-spiral potential varies. An additional novelty of this work in comparison with previous studies is that we do not confine ourselves to the study of barred-spiral systems with the end of the bar close to corotation. Morphological features of the bar pronounced in even slower rotating models will be discussed in Tsigaridi & Patsis (2013b) (Paper II). In cases we want to investigate the differences introduced in the dynamics when we have a stronger m=2 component in the spiral arms region, we modify appropriately the a_n values of the coefficients of the polynomials that build the Φ_{mc}, Φ_{ms} terms in Eq.(1) and this results to a model with a stronger perturbation. Such models, as well as fast rotating cases, are presented by Patsis & Tsigaridi (2013) (Paper III).

3 THE METHOD

The steps we follow in order to identify the dynamical mechanisms giving rise to the various morphological features, which we en-

counter as we vary the pattern speed, can be schematically summarized as follows:

(i) We calculate the stellar response by imposing the model potential to a set of initial conditions.
(ii) We isolate in the density maps of the response models the regions, where we observe the features we want to analyse.
(iii) We study the statistics of the Jacobi constants (E_J, hereafter called the energies) of the particles participating to the formation of the specific morphological feature under study.
(iv) At energies, where we find many particles contributing to the local surface density in the region of the feature under study, we investigate the possible orbits of these particles. We consider the $y = 0$ surface of section for orbits intersecting it with $\dot{y} > 0$ and in cases it was needed we considered also the corresponding $x = 0$ surface of section with orbits intersecting it with $\dot{x} > 0$. Then we calculate orbits on a dense grid of initial conditions on the surfaces of section, covering the allowed phase space at this E_J, as it is defined by the curves of zero velocity. Viewing the location of the initial conditions of these orbits on the surfaces of section we practically know if the orbits behave as regular or chaotic. If an orbit from a chaotic sea starts in reality on a tiny stability island, not discernible in the figure, this will not affect our conclusions. At any rate we are interested about orbits integrated for a given time interval (see section 4.3 below).
(v) By calculating the full tree of characteristics (see e.g. Contopoulos & Grosbøl 1989) for each model and the stability curves (i.e. the Hénon (1965) index, as a function of E_J) of every family, we know the location and the stability of the periodic orbits at each E_J at least until multiplicity three. Then, from the calculated extent of the stability islands around the stable periodic orbits (hereafter "p.o."), from the structure of the asymptotic curves associated with the unstable p.o. and from the sticky zones in the phase space, we estimate the contribution of the various dynamical mechanisms to the formation of the spiral arms, the bar, the rings or any other structure that eventually appear in the model.

The details of this procedure become clear in the following example, which can be considered as the "general" case, in the sense that it harbours versions of all dynamical mechanisms we encountered in all studied models of this gravitational potential with different pattern speeds.

4 THE GENERAL CASE

We run more than 20 response models for pattern speeds Ω_p in the range $10 < \Omega_p < 40$ km s^{-1} kpc^{-1}. For all of them we studied their orbital structure. All of them developed some barred-spiral morphology, the exact structure of which was changing as we varied Ω_p. E.g. the pitch angle of the response spiral or the extent of the bar depended on Ω_p. The reason for the change of the response morphology was the activation of different dynamical mechanisms for different pattern speeds. Nevertheless, despite the differences, all of the response morphologies are barred-spiral. For the case we consider as "general" we take Ω_p=15 km s^{-1} kpc^{-1} and we use about 10^6 test particles. The generality of the case results from the fact that in the formation of the barred-spiral morphology of the particular response model, as we will see, participate all of the main dynamical mechanisms we encountered by studying the dynamics of potential (1) rotating with different Ω_p.

We impose the full potential $\Phi(r, \varphi)$ (Eq. (1)) to a set of initial conditions, which are randomly distributed homogeneously on a disc of radius $r = 11$ kpc. The system in each model rotates with its pattern speed Ω_p, in our case 15 km s^{-1} kpc^{-1}. To the particles were given initial velocities v_0, either such as to secure circular motion in the axisymmetric part of the potential $\Phi_0(r)$, or velocities with a certain dispersion around v_0. By giving velocities close to the circular velocity in $\Phi_0(r)$ and integrating orbits in $\Phi(r, \varphi)$ the system chooses by itself the orbital families to populate. In general we observe that the basic morphological features of the response models do not change as the initial dispersion of the velocities increases. However, they become less sharp, as we will see below.

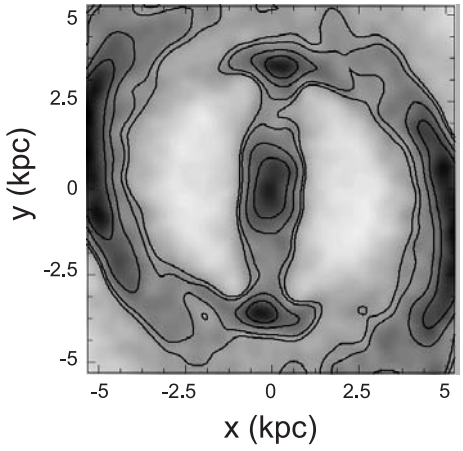

Figure 4. The inner bar-spiral morphology of our model. Note the inner boxy isophotes of the bar. Darker shades correspond to denser regions.

The initial conditions are integrated for 10 system rotations using a standard 4th order Runge-Kutta scheme. The equations of motion are derived from the Hamiltonian

$$H \equiv \frac{1}{2}\left(\dot{x}^2 + \dot{y}^2\right) + \Phi(x, y) - \frac{1}{2}\Omega_p^2(x^2 + y^2) = E_J \qquad (2)$$

where (x, y) are the coordinates in a Cartesian frame of reference rotating with angular velocity Ω_p. $\Phi(x, y)$ is the potential (1) in Cartesian coordinates, E_J is the numerical value of the energy and dots denote time derivatives. There is an initial time interval in the runs of the models, during which the total perturbation increases from 0 to its total amplitude.

The isocontours of the effective potential $\Phi_{eff} = \Phi - \frac{1}{2}\Omega_p^2 r^2$ are given in Fig. 2a, where we indicate the location of the Lagrangian points L_1, L_2 (unstable) and L_4, L_5 (stable). For L_1 and L_2 we have $E_{L_{1,2}} = -27772$ (in units of km^2 s^{-2}), while their coordinates are $(x, y) = (\mp 0.042, \pm 8.856)$ respectively. The system rotates counterclockwise.

Models starting with the particles in pure circular motion in the axisymmetric component Φ_0 and models with velocity dispersions up to 20% of the circular velocity in the tangential and up to ±45 km s^{-1} in the radial direction, do not show any qualitative difference in their response morphology and in general are similar among themselves.

In the current case the response model with circular initial velocities of the particles is presented in Fig. 2b, while one with initial tangential velocities as in Fig. 3 and a radial velocity dispersion about ±40 km s^{-1} is presented in Fig. 2c. The initial tangential velocities are given to the particles by adding or subtracting randomly to v_0 a velocity term in the range up to $0.2 \times v_0$. In Figs. 2b,c darker regions correspond to higher surface densities. Both responses are very similar and are characterized by an inner barred-spiral structure and an extension of the spirals to larger radii as weaker fea-

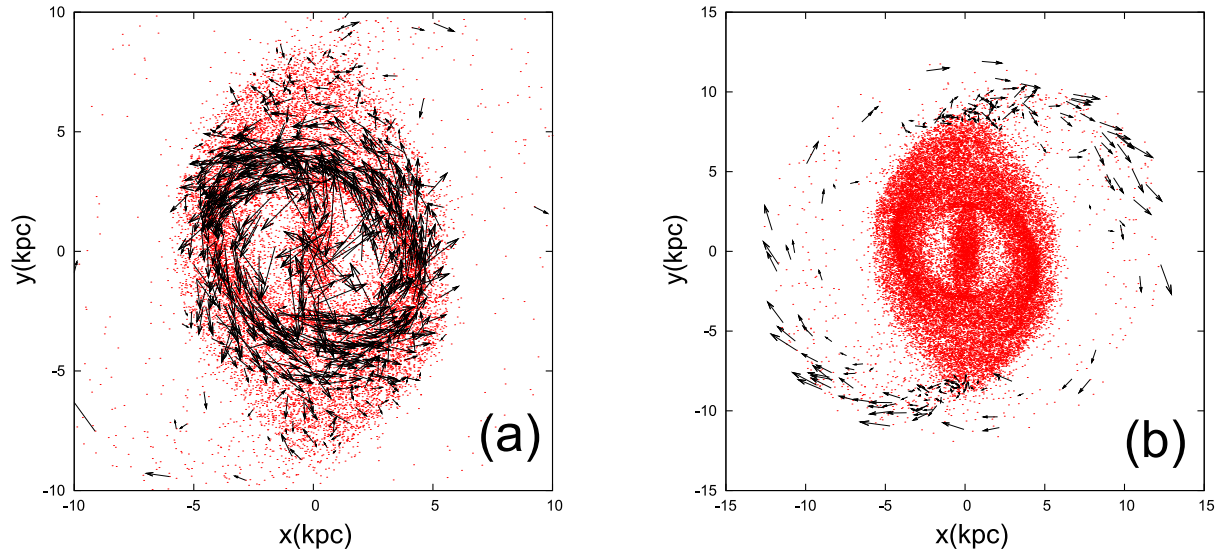

Figure 5. (a) The flow in the region of the bar and the inner spirals. (b) The flow along the outer fainter arms. The size of the arrows is scaled so that we can qualitatively understand the flow in the two regions.

tures. The models are presented as they appear after 10 pattern rotations. In models with higher dispersion of velocities we find at the end of the simulation more particles in the spiral arms region beyond corotation. The response of the model we observe in Fig. 2 does not change if we continue to integrate the orbits of the particles for more than 10 pattern rotations. Particles that "escape" are substituted by particles at random positions and initial velocities according to the initial set up.

The response morphology is characterized firstly by the presence of a bar. The dynamics of the bar, in all models with Ω_p = 15 km s^{-1} kpc^{-1} we examined, follows in general the standard x1 flow with stable p.o. of elliptical shape aligned almost along the major axis of the bar (Contopoulos & Grosbøl 1989). So we will not present the orbits reinforcing the bar here. We only note a boxiness of the central isophotes in the bar region (Fig. 4). The orbital dynamics leading to this feature are in all cases the same, but they are more pronounced in models with even lower Ω_p. This and other deviations from the standard "x1-flow" in the bar region will be presented in paper II, where we discuss exclusively slow rotating patterns.

Beyond the bar we observe a symmetric set of spirals with an inner part (its arms are indicated with "A" in Fig. 2c) and an outer one (indicated with "B"). The shape of the isophotes point to a clear local minimum of the spirals in the response density around $7 < r <$ 9 kpc, i.e. close but inside corotation (cf. with Fig. 2a). The outer set of arms in the response models ("B") is fainter, despite the fact that initially we considered the test particles being homogeneously distributed in the disc of the model.

By plotting the velocity field for snapshots of the response model, it is clear already after 3-4 pattern rotations that the flow along the spiral arms changes as the radius increases. In Fig. 5a we depict the velocity field by focusing in the bar region and in the region including the part "A" of the spiral arms (Fig. 2b), while in Fig. 5b we give the velocity field in the outer parts of the model. The difference in the two flows is conspicuous. On one hand, in Fig. 5a we have a flow around the centre of the system in the sense of its rotation (counter-clockwise). We notice that the vectors become disordered as we approach corotation. On the other hand in Fig. 5b the flow is along the faint spiral arms. To a certain degree the situation resembles the flows given for normal (part "A" of the spiral) and barred-spiral galaxies (part "B") respectively as described by Patsis (2009). However, both flows are associated with the spiral arms of the response model. This is an important result, because it shows that two different flows coexist in the same model and cooperate to structure a uniform response morphology. In order to study the orbits of the particles that participate in the formation of the arms we divide the response model in concentric rings. The spiral arms of the model start close to the end of the bar (part "A"), while the faint extensions extend beyond $r > 8.2$ kpc (part "B").

4.1 Segments of spiral arms

As we see in Fig. 6a the spiral arms can be morphologically divided in four parts by the concentric rings we draw. Within each annulus the spiral arms are the denser feature. The underlying model is the one in Fig. 2b. The annular regions are separated by circles drawn successively at $r = 3.4, 5, 6.6$ and 8.2 kpc. These radii have been chosen by careful inspection of Figs. 2 and 5 and correspond to radii at which we observe changes in the morphology and the flow of the model. Darker shades correspond to denser regions. The contrast of the image is chosen such as to reveal details of the spiral arms up to the radius of L_1, L_2. The shape of the spiral arms for $r > 8.2$ (i.e. starting slightly inside the L_1, L_2 radius) is inferred from the overplotted isocontours. For all particles in each region we perform statistics in their energies. The distribution of the energies are given in Figs. 6b to e. As a next step, we consider in all cases the E_J value that appears most often in each annulus (the mode of the histogram) and we investigate the orbital dynamics in our model for this energy. It is expected that this will characterize to a large degree the orbital dynamics of the arms in the corresponding region, since the majority of the particles in the annulus will be close to the mode E_J value. A verification of the result is done by overplotting the orbits we find to dominate at this E_J on the response density map of our model, in order to check if and how an orbit reinforces the morphological feature we study. In cases we find that there is significant contribution in another E_J range apart

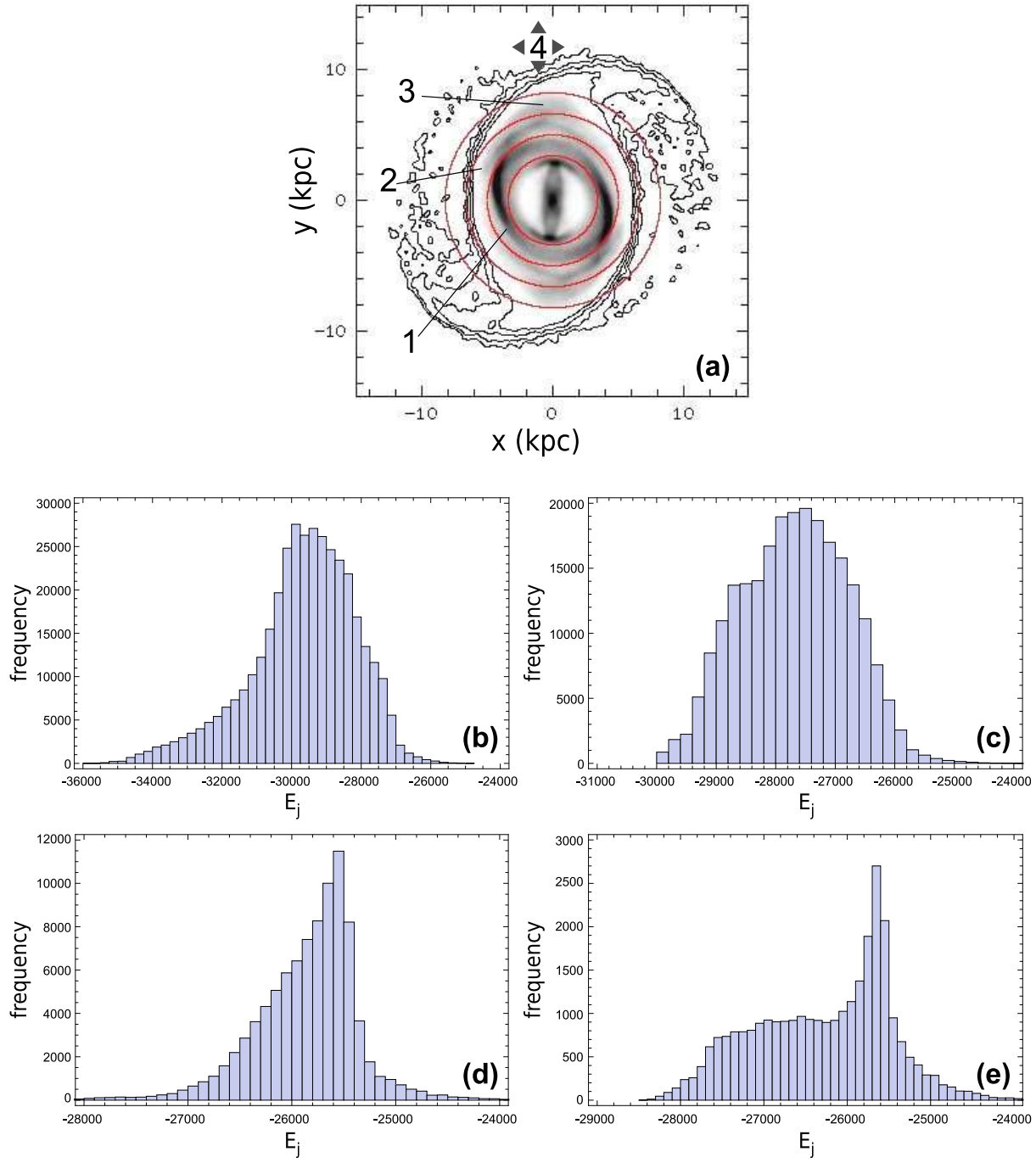

Figure 6. (a) The division of the arms in four regions by drawing four concentric circles at radii $r = 3.4, 5, 6.6$ and 8.2 kpc. From (b) to (e) we give the energies' distribution in the regions $3.4 < r < 5$ ("1"), bin size 250, $5 < r < 6.6$ ("2"), bin size 200, $6.6 < r < 8.2$ ("3"), bin size 100 and $r > 8.2$ ("4"), bin size 100, respectively.

from the mode value, we repeat our analysis in this energy range. The results of this investigation are described below.

4.2 Region "1"

The mode of the distribution of E_J in region "1" is at $E_J = -30000$ (Fig. 6b), while there are significant contributions in the range $-30250 < E_J < -29500$. In all these energies order dominates and the surfaces of section are characterized by the presence of big islands of stability around the stable periodic orbit x1. The $(x, \dot{x})$ surface of section for $E_J = -30000$ is given in Fig. 7a.

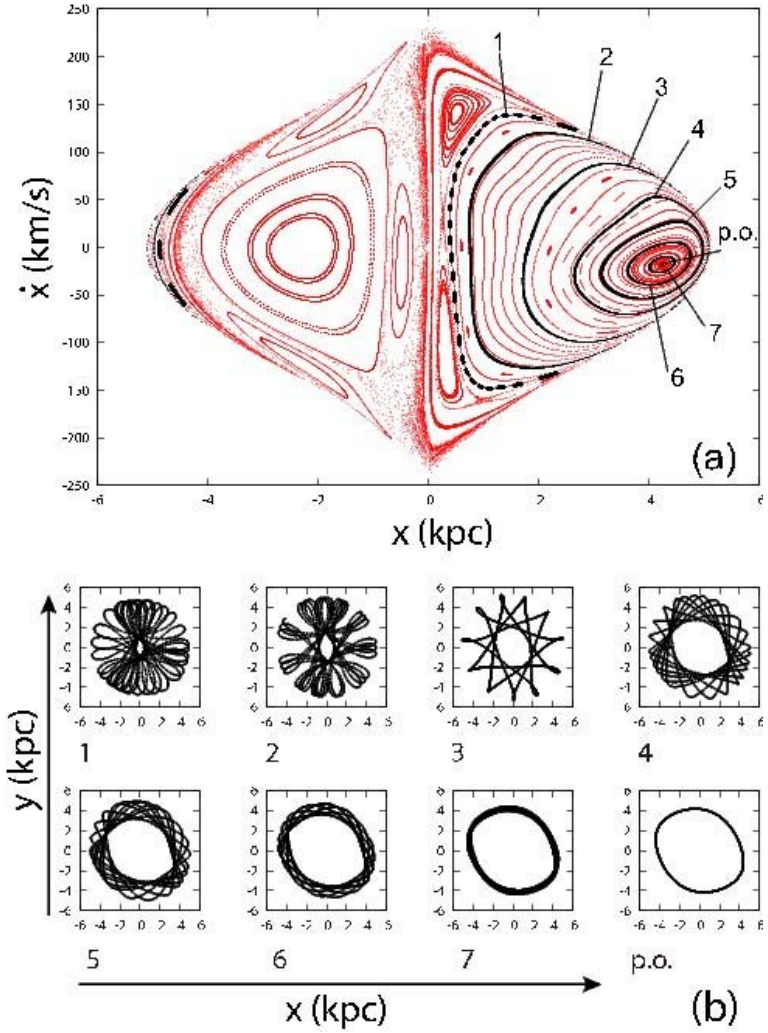

Figure 7. (a) The surface of section for $E_J = -30000$. (b) Successive quasi-periodic orbits corresponding to the invariant curves labelled with the corresponding number in (a). The p.o. x1 is given in the lower right panel. Only the orbits in panels 5, 6 and 7 reinforce the spirals in region "1".

By viewing this landscape we conclude that the orbits that support the inner strong spirals, which appear immediately beyond the end of the bar in the model, can only be quasi-periodic orbits around the stable p.o. x1. Chaos is almost absent for $x > 0$ (Fig. 7a). The location of the p.o. is indicated by an arrow labelled "p.o." in Fig. 7a. Its shape is given in the lower right panel of Fig. 7b. The available orbits in the range $-30250 < E_J < -29500$, as inferred from the surfaces of section, combined with the velocity field of the model we presented in Fig. 5, strongly indicate the presence of a "precessing ellipses mechanism" (Patsis 2009) associated with the spiral arms. In this energy range the x1 orbits are not any more almost aligned with the major axis of the bar, but precess as the energy varies. By plotting successive elliptical x1 p.o. with $-30250 < E_J < -29500$ (Fig. 8), it is evident that they precess in such a way as to support the spiral arms. From Fig. 8 we conclude also that the quasi-periodic orbits supporting the spiral arms in region "1" should not considerably deviate morphologically from the p.o., since the p.o. by themselves reproduce the pattern that supports the spirals. The populated quasi-periodic orbits should correspond to the smaller invariant curves around the x1 p.o. Indeed, only the orbits in panels 5, 6 and 7 in Fig. 7b reinforce the spirals. They correspond to the innermost three invariant curves around the p.o. in Fig. 7a. The quasi-periodic orbits in the panels that correspond to the other invariant curves of Fig. 7a do not support the spiral arms. It is known that considering quasi-periodic orbits with the same E_J value on different sets of invariant curves around the same p.o. can lead to different response morphologies (Patsis 2005). It is also known that the shape of a p.o. is in general different from the shape of the structure it supports by being part of its backbone (Patsis 2005).

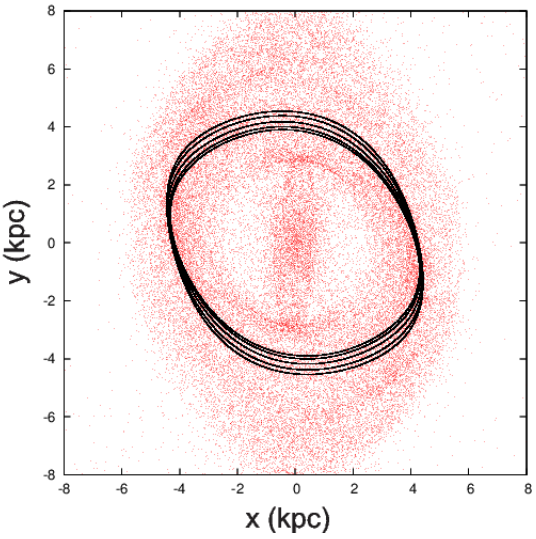

Figure 8. x1 family orbits at energies from inside to outside −30500, −30300, −30000, −29700, −29500. They come very close, without intersecting each other, in the regions of the spiral arms.

4.3 Region "2"

In Figs. 2b,c we observe that the strong spirals continue in region "2" (Fig. 6a) as thinner features with a different pitch angle. Following the same procedure as before, we examine the E_J distribution of the particles in annulus "2" (Fig. 6c). The structure observed in region "2" is reinforced by particles mainly in the range $-28800 < E_J < -26600$ having a mode at $E_J = -27770$. This means that we have a contribution from particles with energies around the energies of the unstable Lagrangian points ($E_{L_{1,2}} = -27772$) and close to it. The fact that we find in region "2" also particles with $E_J > E_{L_{1,2}}$, located at radii smaller than that of $L_{1,2}$, raises the question of a possible contribution to the observed local response surface density maxima in region "2" by the "hot orbital population".

In our investigation we use also another useful tool for the study of orbital dynamics of galaxies, which is the (E_J, x_0) diagram of the characteristics of the main families (Contopoulos 1970). In our case the characteristics of the central family x1 and all other main simple periodic families for $-30000 < E_J < -24000$ are given in Fig. 9. Black parts along the drawn curves indicate stability, while grey (red in the online version) instability Family x1 becomes unstable for $E_J > -29316$, bifurcating two 3:1 simple periodic families. As we see in Fig. 9 the characteristics of the two new families follow complicated paths reaching a maximum for $E_J \approx -28100$. Together with x1 and the characteristics of other families that are inversely bifurcated from x1 at larger energies (indicated as "4/1" in Fig. 9), form a bundle of characteristic curves that fill the largest part of the characteristic diagram between $-29000 < E_J < -28400$. Along all these curves the morphology of

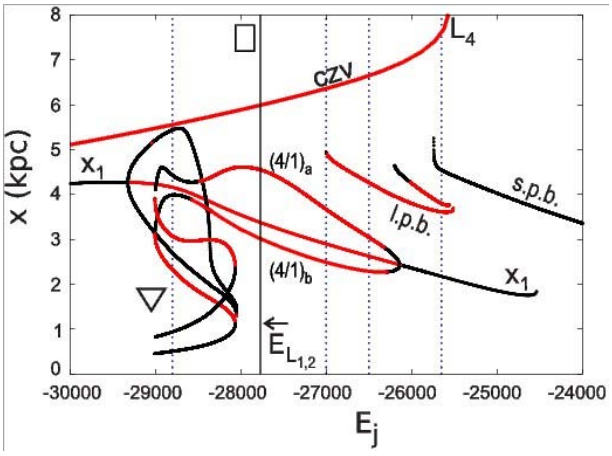

Figure 9. The characteristic curves of x1 and the main families of simple periodic orbits for $E_J > -30000$. The vertical lines indicate the E_J locations at -28800, -27772, ($E_{L_{1,2}}$), -26500 and -25650. Black parts indicate stability, while grey (red in the online version) instability.

the periodic orbits changes gradually from 3:1 to 4:1 type as energy increases. This change of morphology designates the passing from the 3:1 to the 4:1 resonance region. We indicate this change schematically by drawing a triangle close to the vertical line at $E_J = -28800$ and a rectangular to the left of the $E_{L_{1,2}}$ energy. All p.o. are asymmetric. We note that the initial conditions of the p.o. have in general non-zero initial velocities. A (E_J, x_0) diagram depicts projections of the characteristics. Thus, in Fig. 9 we do not have real intersections of the curves, except at the bifurcations points.

The evolution of the phase space in the region "2" is depicted in Fig. 10. From top to bottom we have the $(x, \dot{x})$ surfaces of section for $E_J = -28800$ (a), -28000 (b), and -27000 (c) respectively. They are characterized by the presence of a chaotic region that seems to be included within a KAM curve and is roughly extending in the area $(\Delta x \times \Delta \dot{x}) \approx (2, 6) \times (-100, 100)$. We call it "the chaotic lake" in order to facilitate the description of the figures. As we increase the energy we encounter in it both stability islands and chaos until $E_J \approx -28100$. A typical example is the one in Fig. 10a. For larger energies we observe in this region only chaos surrounded by a KAM curve as in Fig. 10b. The same happens also for $E_J = -27000 > E_{L_{1,2}}$ (Fig. 10c). However, from this energy on, by starting integrating orbits in the chaotic lake we have in addition consequents appearing to the left and to the right of the central region of the $(x, \dot{x})$ surface of section. This is a consequence of the opening of the curves of zero velocity for $E_J > E_{L_{1,2}}$. The chaotic lake splits in three parts. In Fig. 10c we observe consequents to the left and to the right of the central part. Regions appearing depleted from consequents represent orbits that follow immediately long journeys away from the bar-spiral region and are discussed in detail below.

In order to find out which is the dominating orbital behaviour at a specific E_J and check what is its relation to the observed structure in the region we examine, we have taken initial conditions on a dense grid and we have integrated orbits for time corresponding to 8 pattern rotations. We will refer hereafter to this time interval as T_8. This time interval is safe against secular evolution, for applying the Hamiltonian approximation in modelling the galaxy. In addition T_8 is enough for building stable structures as we empirically realize from our response models. In that sense we are not looking for orbits with regular behaviour over a Hubble time or more, but

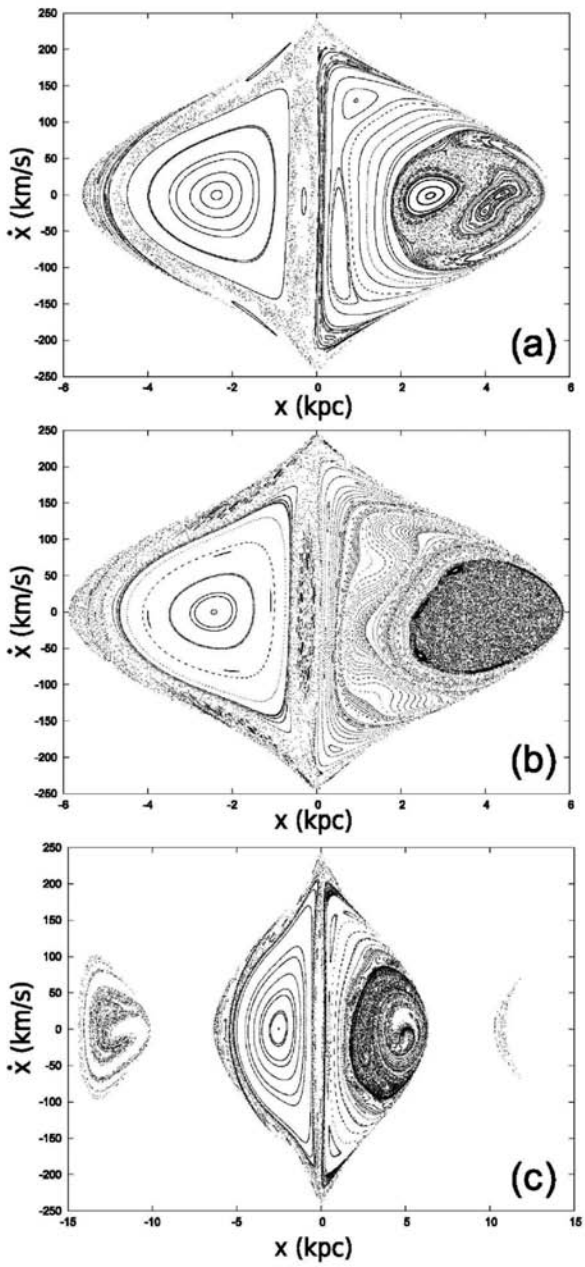

Figure 10. Three $(x, \dot{x})$ surfaces of section at energies in which we find particles supporting the continuation of the spiral arms in region "2" **(see Fig. 6a)**. In (a) $E_J = -28800$, in (b) $E_J = -28000$ and in (c) $E_J = -27000$.

for many orbits which have similar morphologies, due to stickiness effects, within T_8. By plotting these orbits we could easily realize that only orbits from the chaotic lakes in $-28800 < E_J < -26600$ bring particles in the spiral arms region.

The orbital dynamics changes as energy increases towards $E_{L_{1,2}}$. In Fig. 10a we have $E_J = -28800$. As we see in Fig. 9 the left vertical line crosses the characteristic of all families of periodic orbits at this energy, thus they are present on the surface of section. In this energy, the x1 orbit at $(x, \dot{x}) \approx (4.16, -9.5)$, is unstable. However, it is surrounded by invariant curves together with two stable p.o. bifurcated at the transition of x1 from stability to instability. Totally we have six stability islands corresponding to

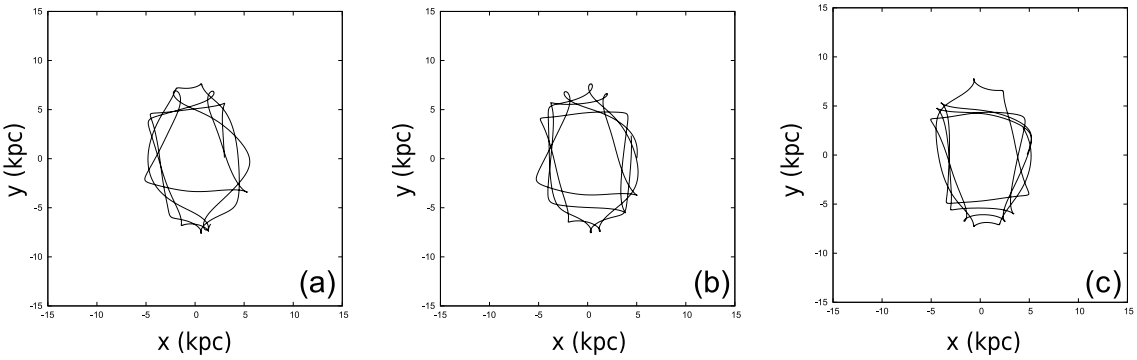

Figure 11. Three characteristic orbits at $E_J = -28000$ that enhance the surface density in region "2" (Fig. 6a). Their segments, which are roughly parallel to the x-axis reinforce also the bifurcation of the spiral arms appearing in the region.

the stable p.o. found from the intersections of the left vertical line in Fig. 10a. All of the stable p.o. have triangular shapes. None of them helps in the formation of the structure we observe in region "2". We found that contributions to the spiral arms structure are coming only from the quasi-periodic orbits surrounding both x1 as well as the two bifurcating families, and from the chaotic orbits from the sticky zones surrounding the other two 3:1 stability islands existing in the chaotic lake (one at its right border and another around $(x, \dot{x}) \approx (2.75, 0)$). These orbits are also reinforcing to some degree the bifurcating features from the spirals that tend to form a pseudoring in region "2". However, more significant contribution to the structures in this region is coming from particles with larger E_J close and beyond $E_{L_{1,2}}$.

For $E_J = -28000$ (Fig. 10b) there are no stability islands in the chaotic lake any more. Particles with this E_J do not belong to the orbital population visiting both the bar and the spirals because the value of $E_{L_{1,2}}$ is larger than -28000. The integration of a dense grid of initial conditions over the whole $(x, \dot{x})$ surface of section clearly shows that dense surface density features in region "2" are supported by orbits having mainly a 4:1 resonance character, with segments roughly parallel to the x-axis. Such orbits reinforce the bifurcations of the arms that extend also in region "1". Three such orbits are presented in Fig. 11. These are chaotic orbits *inside corotation*, that support a spiral pattern. Their similarity with the orbits proposed to be associated with the spiral arms of NGC 1300 by Patsis et al. (2010) indicate that "chaotic spirals" inside corotation may be present in a larger class of barred-spiral systems. Orbits with a 3:1 character exist in the system but are not populated in the response model. If they were populated, they would not enhance but destroy the spiral structure.

In conclusion in region "2" the segment of spiral arms in it is supported mainly by chaotic orbits with $-28000 < E_J < E_{L_{1,2}}$. Their morphology resembles orbits of 4:1 type. More interesting is the fact that there is also a contribution to the segment of the spiral arms located in region "2" from particles with energies beyond the E_J values of the unstable Lagrangian points $E_{L_{1,2}}$, despite the fact that L_1 and L_2 are located at a larger radius. This indicates an important role of the hot orbital population of particles visiting both the bar and the arms region, for the overall dynamics and morphology of the model. This will become evident in the following sections.

4.4 Contribution to regions "2" and "4"

Fig. 10c shows a $(x, \dot{x})$ surface of section at $E_J = -27000$, which is typical for energies immediately beyond $E_{L_{1,2}}$. A closer study of the dynamics at this energy is necessary not only for the dynamics of region "2" (Fig. 6a), but also for the dynamics of the outer part of the spirals extending in region "4", i.e. for $r > 8.2$ kpc. We present our results at this point before going to the discussion of region "3". The importance of the dynamics at energies close to $E_J = -27000$ is evident in Figs. 6e,c. In Fig. 6e we observe that we have a significant contribution of particles with energies in the interval $-27772\ (= E_{L_{1,2}}) < E_J < -26000$. Altogether we find more particles with these energies in the outer spirals, than in energies close to the mode of the distribution in Fig. 6e at $E_J = -25650$, because of the long tail of the histogram to the left of its mode. The surfaces of section in the interval $-27772 < E_J < -26000$ are similar to the one for $E_J = -27000$ (Fig. 10c), so we focus on it.

In comparison with Figs. 10a,b, in Fig. 10c we observe in the $(x, \dot{x})$ surface of section two more regions with consequents, on the sides of the central one, as expected, since we are now beyond the energy of the Lagrangian points $L_{1,2}$. The chaotic lake communicates with them. The diagram of the characteristics (Fig. 9) tells us that for $E_J = -27000$ we have three unstable simple-periodic orbits and a member of the family of the long period banana-like orbits (Contopoulos & Grosbøl 1989), which is designated as "lpb" in the figure. This family is found to be stable at the lowest energy we find it and then is mainly unstable. We find also long period banana-like orbits along another branch of a characteristic in Fig. 9 for $-26200 \lessapprox E_J \lessapprox -25500$ with a stable part for its lowest energies. The initial conditions of the p.o. of all these families are located in the chaotic lake in Fig. 10c. Their morphology is given in Fig. 12. The rectangular type orbits are all unstable, while the long period banana-like orbit at this energy is stable. However, the stability island around it is tiny and not easily discernible in the surface of section without zooming.

Focusing into the region of Fig. 10 with $0 < x < 6.6$ (Fig. 13) we imposed a grid of initial conditions on the surface of section and we integrated 1027 orbits for time T_8. By overplotting these orbits on the response model we realized that only non-periodic orbits from the chaotic lake reinforce the part of the spiral structure in region "2", and/or the spirals extending beyond 8.2 kpc. Orbits outside this area in Fig. 13 are irrelevant to the observed structures and are not populated in the response model.

In Fig. 13a we point with arrows to the initial conditions of the simple periodic orbits and we indicate them with their names. The

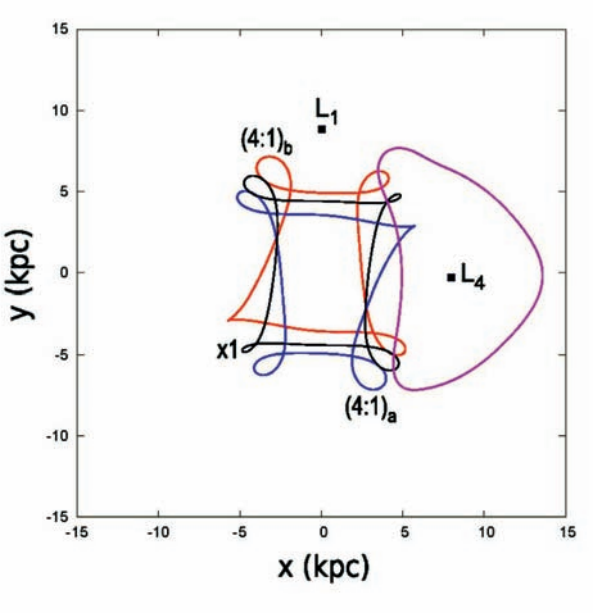

Figure 12. The morphology of the simple periodic orbits we found in the system for $E_J = -27000$. The black orbit is the x1 representative at this energy, while the other two rectangular like orbits are those indicated by $(4:1)_{a,b}$ in Fig. 9. All of them are unstable. The orbit at the right side of the figure is a long period banana-like orbit, stable at this energy.

rectangular symbol next to the initial conditions of x1 indicates its morphology character (Fig. 12). The banana-like stable orbit "lpb" is surrounded by a tiny island of stability. The heavy dots plotted in the chaotic lake correspond to $(x_0, \dot{x}_0)$ initial conditions on the grid of integrated orbits, which support the spirals in region "2" or/and beyond 8.2 kpc (region "4"). In this set of initial conditions one can apply the algorithm suggested by Chatzopoulos et al. (2011) to classify their morphologies. However, in the present case, the orbits relevant to the features we study can be divided by eye in two classes. (a) Those which spent a considerable time in the bar region and demonstrate a morphology which can be vaguely described as having a "4:1 resonance" character and (b) those that follow a path bringing them directly beyond corotation through the L_1 or L_2 windows. Typical examples of the first and second class are given in Fig. 13b and Fig. 13c respectively. All of these orbits belong to the "hot orbital population" and visit both region "2" and the disc beyond the corotation region. However, not all orbits belonging to the first kind go through the L_1 or L_2 gates during the integration time T_8, but they do so in later times. In Fig. 13a heavy black dots correspond to orbits of the first class, while grey (green in the online version) to the second.

In Fig. 10c, as well as in Fig. 13a we observe regions depleted from consequents. These are not really empty regions, but represent orbits that perform long loops away from the central area of the model. Since our potential is not well defined for $r > 12.5$ kpc practically the "white" regions indicate the presence of orbits that reach distances larger than 14 kpc. These orbits will be discussed in more detail in Patsis & Tsigaridi (2013) (paper III), where models with $\Omega_p > 15$ km s^{-1} kpc^{-1} are presented.

Careful inspection of Fig. 13a shows that the grey (green online) heavy dots are always found in these "white" parts; not only in the main white region at the right part of the surface of section, but also in "white stripes" that cross the dense regions of the chaotic lake. The same analysis has been done in the left region of Fig. 10c, giving similar results.

We notice that in the present model the "hot orbital population" does not bring material beyond corotation from an envelope just surrounding the bar (as it was done in the model for NGC 4314 described in Patsis (2006)), but from a larger disc region around the bar. This is expected since $R_c/R_b \approx 2.9$, thus we have enough space on the disc between the end of the bar and the Lagrangian points. The dynamics of the model described here shapes now also the disc region surrounding both the bar and the inner spiral. As mentioned elsewhere (Patsis & Kalapotharakos 2011) these dynamics lead to morphologies similar to what is observed in some grand design galaxies like NGC 1566 and NGC 5248, where two sets of bisymmetric spirals co-exist. In Fig. 14 we overplot two characteristic orbits with $E_J = -27000$ on the response model, so that their contribution to the shaping of the outer boundary of the disc region inside corotation and to the outer spiral arms becomes conspicuous.

Having calculated the exact location of the simple periodic orbits, we can calculate the asymptotic curves (manifolds) of the unstable periodic orbits on the surfaces of section. This will allow us to investigate in what degree a manifold occupies a region in the surface of section where the orbits follow morphological patterns with common features if integrated for time T_8. In our case we want to examine if a region occupied by a manifold separates regions in which the two different classes of orbits (Fig. 13b and Fig. 13c) dominate. In Fig. 15 the background (light grey dots - red in the online version) is the $(x, \dot{x})$ surface of section in the region of the chaotic lake. The drawn straight lines represent the eigendirections of the unstable x1 p.o. The location of x1 is indicated with a white dot at the intersection of the two lines. The unstable eigendirection is along U_1U_2 and the stable along S_1S_2. The black dots plotted on top of the surface of section in Fig. 15 give the shape of the asymptotic curve associated with the U_1 eigendirection. For the technical details of calculating the asymptotic curves see e.g. Contopoulos & Polymilis (1993). We observe that to a large extent it covers the region of the chaotic lake where we find orbits like the one in Fig. 13b. This can be seen by comparing Fig. 15 with Fig. 13a (note the difference in the scales of the axes in the two figures). The parts of the surface of section not covered by the manifold are those where we find orbits starting inside corotation and almost immediately reinforce the outer spirals as the one in Fig. 13c. There is a good agreement between the empirically calculated initial conditions that demonstrate a 4:1-resonance morphology and the area covered by the x1 asymptotic curve. We have to have in mind that the area occupied by the asymptotic curve is not dense and between the lobes of the manifold there are stripes with consequents not belonging to it. The unstable asymptotic curve of x1 covers the largest part of the area on the surface of section, which contributes to the enhancement of the spiral structure. All chaotic orbits plotted for 8 pattern rotations with initial conditions on this asymptotic curve demonstrate a 4:1 resonance morphology character. These orbits contribute to the density enhancement along the spiral feature in region "2". However, not all of them visit regions beyond corotation within T_8, but they do so in larger times. We find similar results for all other $(x, \dot{x})$ surfaces of section in the $-27772 < E_J < -26000$ range.

The other kind of orbits with $E_J = -27000$ that is important for the dynamics of our model reinforce immediately the outer spirals (labelled with "B" in Fig. 2) without spending much time inside corotation. The particles along these orbits are found in region "4" at $r > 8.2$ kpc (Fig. 6a). If material contributing to the outer spirals is initially in the inner disc region, away from the L_1, L_2 "gates", it

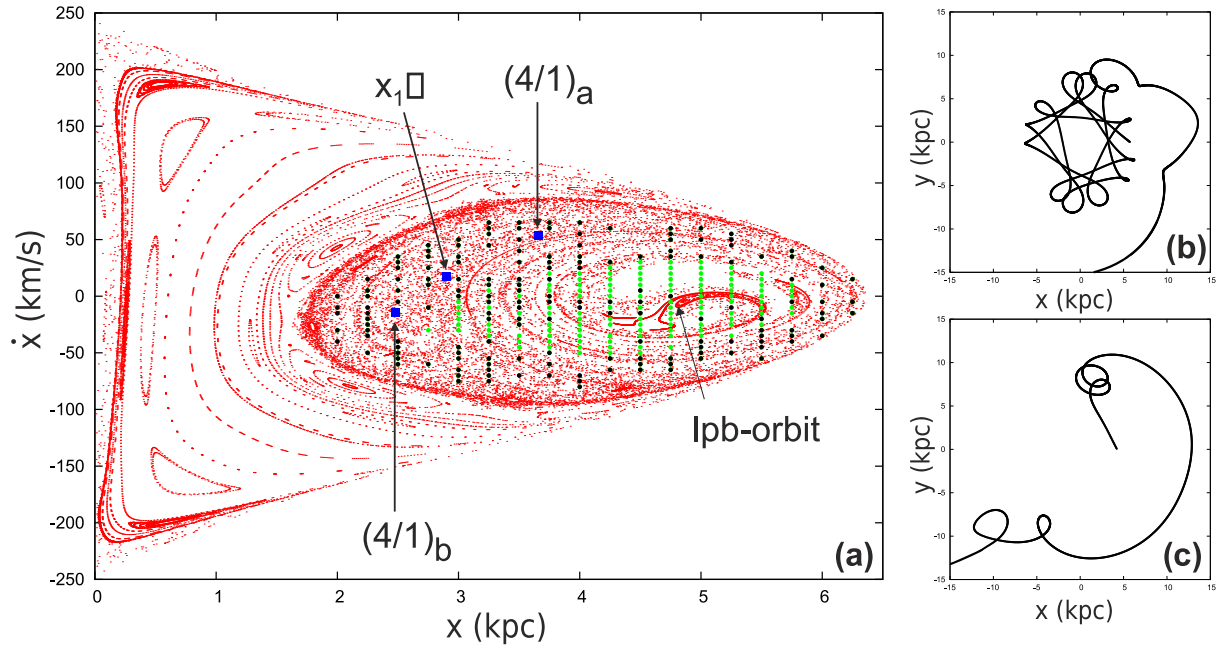

Figure 13. At $E_J = -27000$ ($> E_{L_{1,2}}$) initial conditions of orbits that support the part of the spiral arms in region "2" or the outer spiral arms region during the time T_8 are found in the area of the "chaotic lake" of the $(x, \dot{x})$ surface of section. They are either chaotic orbits which spend a considerable time at radii $r < r_{L_1,L_2}$ or chaotic orbits which go very fast beyond corotation. The initial conditions of orbits of the first kind are denoted with heavy black dots, while those of the second kind with green dots. A typical example of the first kind of orbits is given in (b) and of the second in (c). Arrows indicate the location of the simple periodic orbits on the surface of section.

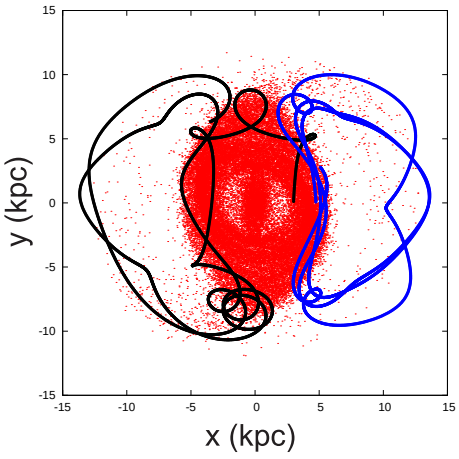

Figure 14. Two typical orbits at $E_J = -27000$, which support the outer spiral and simultaneously shape the borders of the disc region surrounding the inner barred-spiral structure.

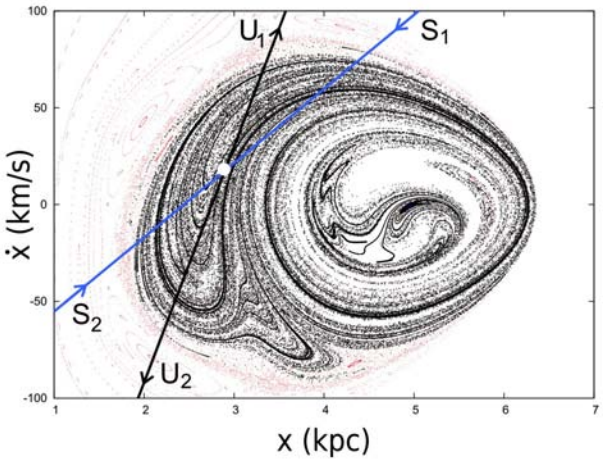

Figure 15. The asymptotic curve associated with the U_1 eigendirection of x1 plotted in the $(x, \dot{x})$ surface of section for $E_J = -27000$. The straight lines represent the U_1U_2 and S_1S_2 eigendirections. The location of x1 (white dot) is at the intersection point of the two lines.

has first to be able to approach the neighbourhood of the unstable Lagrangian points and to have the appropriate energy ($E_J > E_{L_{1,2}}$) and should not be trapped in regular motion around a stable p.o. At $E_J \approx E_{L_{1,2}}$ the main families of simple periodic orbits existing (apart from the family surrounding the L_1, L_2 points, which does not intersect the y=0 axis), are again those depicted in Fig. 12. The energy width ΔE_J at which the 4:1 resonance dominates and affects the morphology of the orbits is the largest among the corresponding ΔE_J intervals of orbits of the $n:1$ resonances with $n > 4$ (see e.g. the stability diagrams in Contopoulos & Grosbøl (1989)).

Like in Fig. 15 also in all other $(x, \dot{x})$ surfaces of section we examined in the energy range $-27772 < E_J < -26000$ we found that the vast majority of the orbits of particles which contribute to the spiral structure are associated with the 4:1 unstable p.o. However, one should examine also the morphology of the orbits in $(y, \dot{y})$ surfaces of section. In these cross sections appear also the PL1 and PL2 families of p.o. (Tsoutsis et al. 2009) surrounding the L_1 and L_2 points. The corresponding to Fig. 10c $(y, \dot{y})$ surface of section is depicted in Fig. 16a. We follow the same procedure of integrating a large number of orbits with initial conditions on a grid. The areas where we find the integrated orbits reaching distances $r > 8.2$ kpc,

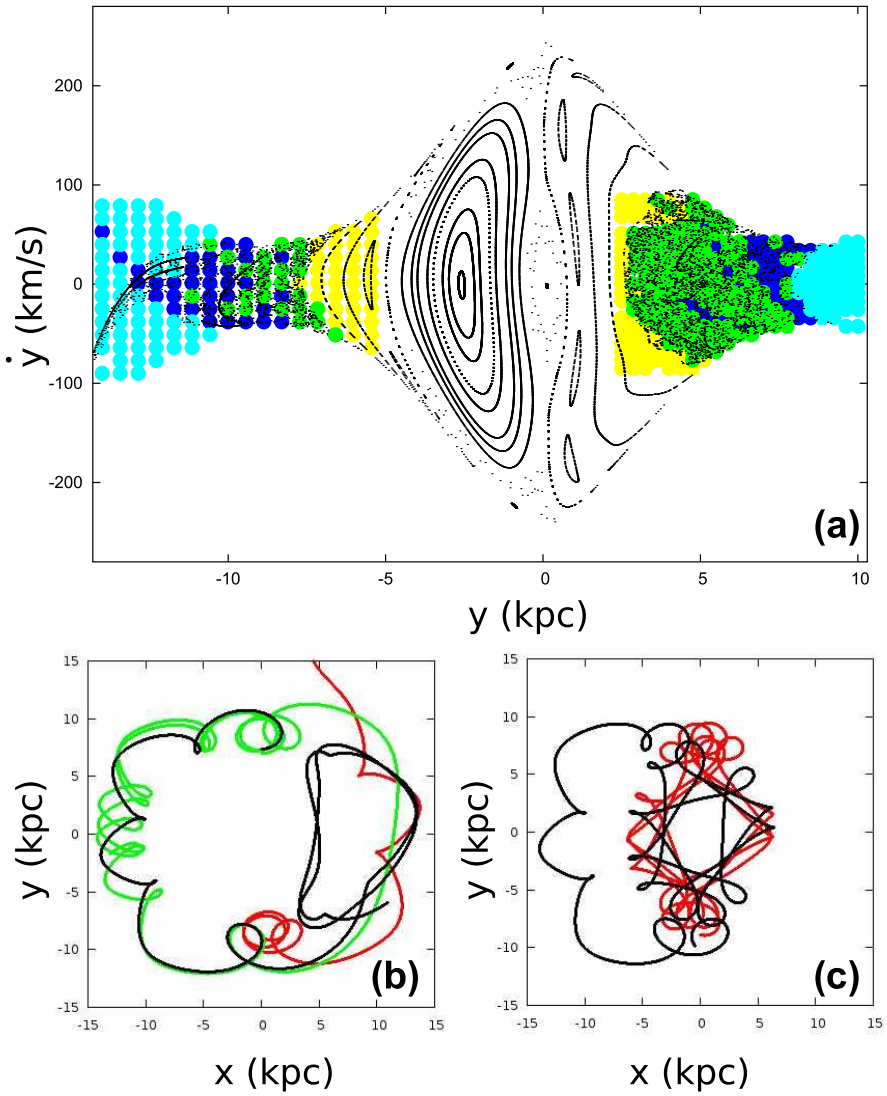

Figure 16. (a) The $(y, \dot{y})$ surface of section for $E_J = -27000$. Coloured areas correspond to initial conditions we have integrated for time T_8. Orbits with initial conditions in the yellow regions, as well as all not coloured areas do not contribute to the morphology of Fig. 2b. Orbits in light blue regions have after short time $r > 12$ kpc and do not reinforce significantly the outer spirals. Dark blue regions represent orbits reinforcing the outer spirals without contributing to the features in region "2". Three such orbits are given in (b). Finally the green regions correspond to orbits either staying for T_8 inside corotation or crossing corotation reinforcing the outer spirals. They have a morphology like that of the two orbits in (c).

and thus being related with the outer spiral structure of our model, are on the left and right sides of Fig. 16a. We find three types of orbital behaviour in these regions. First, orbits which immediately go to distances $r > 12.5$ kpc having a small contribution on the outer spirals of our response model. Their initial conditions are dots coloured with light blue in Fig. 16a. Second, orbits that for time T_8 stay in the region surrounding the inner bar-spiral structure and reinforce practically the outer spirals, like the three orbits given in Fig. 16b. Their initial conditions are coloured with dark blue in Fig. 16a. Finally orbits that stay for a large part of the integration time inside corotation. Their initial conditions on the $(y, \dot{y})$ surface of section are coloured green. 60% of them visit within the time T_8 the outer spirals region. The rest of them do the same at later times. In this category we classify orbits like those depicted in Fig. 16c. The indicated with yellow colour initial conditions correspond to orbits that do not contribute to any structure in our model. No further analysis is needed to conclude that the majority of the orbits with $-27772 < E_J < -26000$ that reinforce the outer spirals within T_8 have partly a 4:1-resonance morphological character. Note that the grid with initial conditions was less dense on the left part.

4.5 Region "3"

The surface density of the spiral in our stellar response model has locally a minimum of its amplitude in the region "3" ($6.6 < r < 8.2$ kpc) of Fig. 6a. This can be observed also in Figs. 2b,c, where the isophotes in the regions close to L_1 and L_2 do not have a spiral arm shape any more. We can speak about a gap or a discontinuity in the spiral arms. The energies of the orbits of the particles are distributed as in the histogram in Fig. 6d. Clearly these particles have energies $E_J > E_{L_{1,2}}$, but are located spatially inside corotation for a time T_8. This means that they belong to the "hot orbital population". The energy range in which we find the particles in region "3" extends over the same E_J values we have to the right of the mode in

the histogram of Fig. 6c. However, the importance of the E_J values increases for larger energies approaching the mode at $E_J = -25650$. Since we are sampling these orbits inside corotation we mainly see in region "3" the tips of the rhomboidal shaped oval area supported by them, which we have already discussed in the previous section (depicted e.g. as background in Fig. 14) close to the Lagrangian points.

4.6 Region "4"

The histogram with the energy distribution of the particles we find at $r > 8.2$ kpc is given in Fig. 6e. The mode of the histogram is at $E_J = -25650$, as is for region "3", clearly indicating that these two regions share to a certain degree a common orbital content. However, as we have already noted, the most significant contribution to the structures formed in region "4" is coming from particles with energies in the interval $-27772 < E_J < -26000$. The orbital dynamics in this range has been presented in section 4.4 and orbits with such energies that visit also the disc region beyond corotation (Fig. 13b,c), reinforce also the outer spirals (indicated with "B" in Fig. 2c).

In addition, in order to investigate all possible orbits that contribute to the outer spirals, we study also the dynamics at the energy of the mode, i.e. at $E_J = -25650$. At this energy the opening in the isocontours of the effective potential around the unstable Lagrangian points is larger and this facilitates the communication between the regions inside and beyond corotation. We have to note that it is a value close, and before, the energy of the stable Lagrangian points L_4 and L_5, at a region where the long-period banana-like p.o. exist (Fig. 9).

The overall structure of the $(x, \dot{x})$ surface of section at $E_J = -25650$ is similar to that of Fig. 10c. However, as we can realize by inspection of Fig. 9, x1 is now stable, since $E_J = -25650$ corresponds to the energy indicated with the rightmost vertical line. From Fig. 9 we conclude that apart from x1 there is, one more stable p.o., with larger x_0 than x1, belonging to the family of short-period banana-like orbits (Contopoulos & Grosbøl 1989) and two unstable long-period banana-like p.o. As regards the pool with orbits available to support the outer spiral arms, it is again the chaotic lake we encountered in smaller energies. All simple periodic orbits we mentioned before are all located for $E_J = -25650$ in this area of the surface of section, which is given in Fig. 17a together with an asymptotic curve, which we will describe below.

In order to classify the initial conditions of the orbits on the surface of section according to their morphology within T_8 and the way they reinforce the structures we study, we followed the same procedure as we did in the previous cases. The question is how well an asymptotic curve of one of the main unstable simple periodic orbits at this energy can separate initial conditions on the surface of section that support the structure we study, from those that do not, when integrated for $t = T_8$. Since x1 is stable in this energy, as main family we consider now the unstable asymptotic curve of the *unstable long period banana-like* p.o. In Fig. 9 it is located in the upper branch of the two unstable branches of characteristic curves intersected by the $E_J = -25650$ line. The results are summarized in Fig. 17a

In Fig. 17a we plot the asymptotic curve in black colour on top of the surface of section which is drawn with red points. The stability islands belong to x1 (the left one) and to the short-period p.o. (the right one). The location of the unstable periodic orbit of the asymptotic curve is indicated with a light blue dot at $(x_0, \dot{x}_0) \approx (3.8, -7.3)$. The "empty" (white) regions on the surface of section belong to orbits that before completing an azimuthal angle $\varphi = \pi$ they visit regions with $r > 12.5$ kpc and thus we stop integrating them, considering them as escape orbits. We observe that the asymptotic curve occupies the largest part of the chaotic lake. This is practically the region where the black points dominate and there we most frequently encounter initial conditions of orbits supporting the outer spirals, without spending much time in the region of the disc with $r < r_{L_{1,2}}$. The morphology of these resemble the orbits in Fig. 16b for $E_J = -27000$. By starting integrating chaotic orbits with initial conditions in the left part of the chaotic lake, roughly to left of the region occupied by the asymptotic curve, we encounter most frequently cases the 4:1-type morphologies (e.g. similar to what we see in Fig. 13b, Fig. 16c).

We note that not all orbits starting in the part of the surface of section depicted in Fig. 17a (roughly the chaotic lake) reinforce the outer spirals within T_8. Firstly we have the two islands of stability containing quasi-periodic orbits around x1 $(x_0, \dot{x}_0) \approx (2.16, 31)$ and around the short-period banana-like orbits at about $(x_0, \dot{x}_0) \approx (4.5, -17)$. These quasi-periodic orbits remain trapped around their stable p.o. One practically adds to them the orbits from the extended sticky regions surrounding their stability islands, especially around x1, as we observe in Fig. 17a. Such orbits are not well-populated in the model. If they were populated they would contribute to the surface density inside corotation (those around x1) and only marginally to the outer spirals (those around the short-period banana-like orbits), since they are located in the outer spiral arms region, but they do not match the spiral arms morphology.

Another typical case, which includes in its morphology the imprints of both the short- and the long-period banana-like orbits, is given in Fig. 17b. This type of orbits exceeds 30% of the orbits we integrated having initial conditions at the regions of the surface of section with $|x| \gtrapprox 8.4$.

In general the amount of hybrid morphologies, i.e. of orbits combining features of different morphological types, is larger at $E_J = -25650$ with respect to surfaces of section with smaller E_J . Such orbits are presented in Fig. 17c,d. They can be found either in the main region occupied by the asymptotic curve or in its tails extending to the left part of Fig. 17a. Exactly because of the large amount of hybrid morphologies, the asymptotic curve separates less efficiently parts of the surface of section, where we find a single type morphology dominating. The blue points plotted in Fig. 17a indicate the location of initial conditions of orbits supporting the outer spirals spending also within T_8 a fraction of time inside corotation following a 4:1-type morphology. Several of them are located in the right part of the figure, occupied by the asymptotic curve.

As a next step we investigated also in this case the orbital dynamics in the $(y, \dot{y})$ surface of section, since the families of p.o. surrounding the unstable $L_{1,2}$ points (PL1 and PL2) does not intersect the $y = 0$ axis. The representatives of this families (with initial conditions $(y_0, \dot{y}_0) \approx (-10.46, 8.8)$ and (5.7, -9.6)) are unstable for $E_J = -25650$. Orbits from their neighbourhood will drift along their unstable eigendirections following trajectories that reinforce the outer spirals. Statistics about the morphology of the orbits have been carried out following an analysis similar to the one for the $(x, \dot{x})$ surface of section and is summarized in Fig. 18a. Open symbols correspond to orbits associated with a banana-like morphology without visiting practically the disc inside corotation (Fig. 18b,c). The chaotic regions we find in the surfaces of section communicate, so starting an orbit close to L_1 or L_2 with $E_J > E_{L_{1,2}}$ there is a large probability to obtain orbits with arcs at $r > r_{L_{4,5}}$. In some cases these orbits remain trapped for some time around L_4 or/and L_5, as in the case of Fig. 18b. Orbits that spend time T_8 (or a consid-

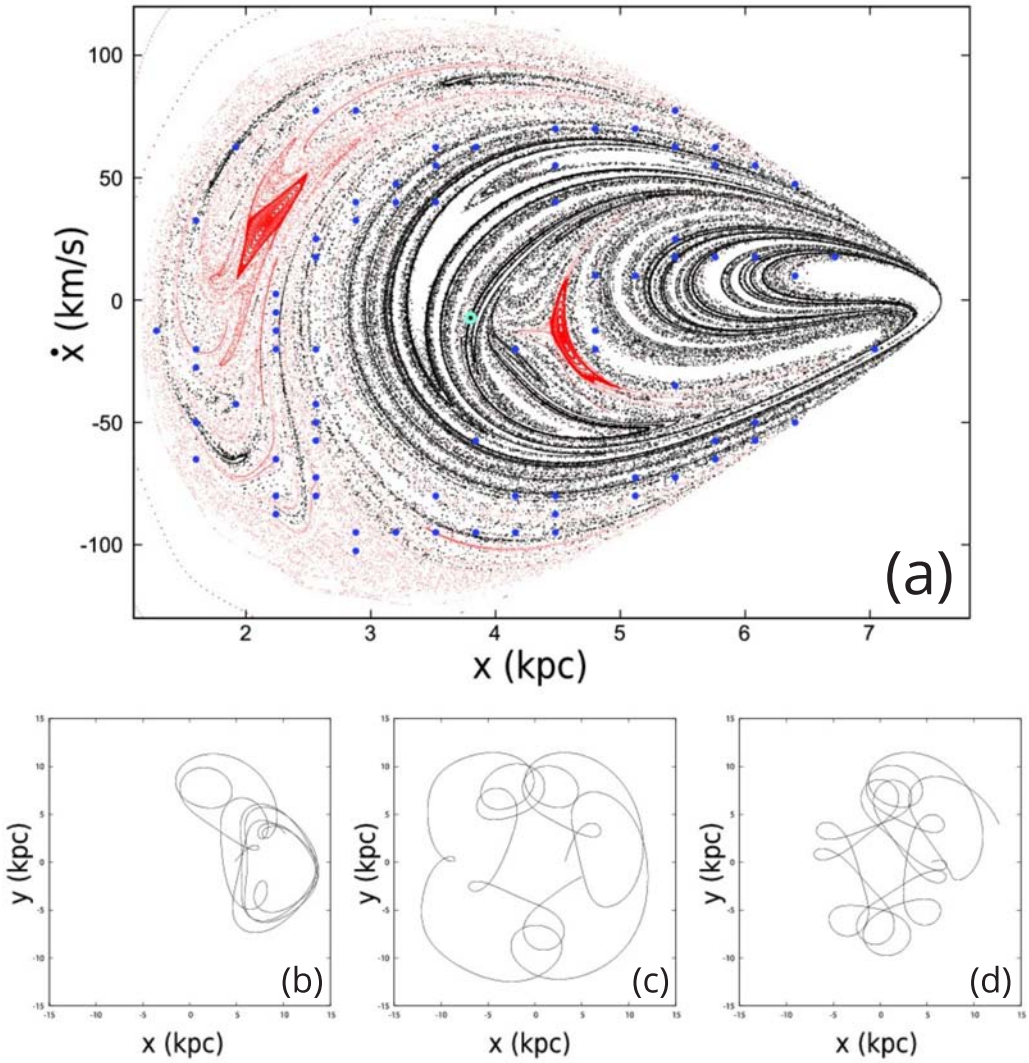

Figure 17. (a) The unstable asymptotic curve of the banana-like p.o. located at $(x_0, \dot{x}_0) \approx (3.8, -7.3)$ plotted in the $(x, \dot{x})$ surface of section for $E_J = -25650$. It occupies a large fraction of the "chaotic lake" area. The dark blue points indicate orbits of the hot orbital population with a 4:1 type morphology within T_8. In (b), (c) and (d) we give characteristic morphologies of the orbits at this E_J .

erable fraction of it) beyond corotation, having always during this time $r < 15$ kpc, are indicated with green open circles in Fig. 18a, while the orbits that practically escape after time less than a pattern period, with light blue ones. Open symbols cover the largest part of the $(y, \dot{y})$ surface of section for $E_J = -25650$.

Nevertheless, even in this surface of section we encounter chaotic orbits with a 4:1-type morphology. Most of them are associated with the sticky region around the last KAM curve of the stable x1 orbit, which has a 4:1-type morphology (like the x1 orbit in Fig. 12, but with larger loops). The initial conditions of these orbits are indicated with smaller black dots, so that the sticky region around x1 can be discernible below them (roughly around (3.5,0) in Fig. 18a). They remain inside corotation for T_8, but they will eventually reinforce the outer spirals in later times. However, there are also hybrid type chaotic orbits sharing a 4:1 and long-period, banana-like morphologies within T_8, as in Fig. 18c,d. In Fig. 18a they are indicated with blue filled circular symbols.

A final interesting remark associated with the statistics of the $(x, \dot{x})$ surface of section at $E_J = -25650$, is that about 25% of the orbits we found supporting to some degree the surface density of the outer spirals in "region 4" do not visit the immediate neighbourhood of L_1 or L_2 within T_8. Such orbits are of the morphology of the two orbits in Fig. 19. Thus, there also orbits supporting the outer spirals without contributing to the surface density close to L_1, L_2.

5 DISCUSSION AND CONCLUSIONS

In the paper we investigated the dynamics shaping a barred-spiral morphology in a response model that we characterized as "general". The "generality" refers to the contribution of mainly four, different, dynamical mechanisms in the building of the observed structure. They become apparent because of the chosen pattern speed that pushes the Lagrangian points far from the ends of the bar ($R_c/R_b \approx 2.9$) and the fact that by construction our model

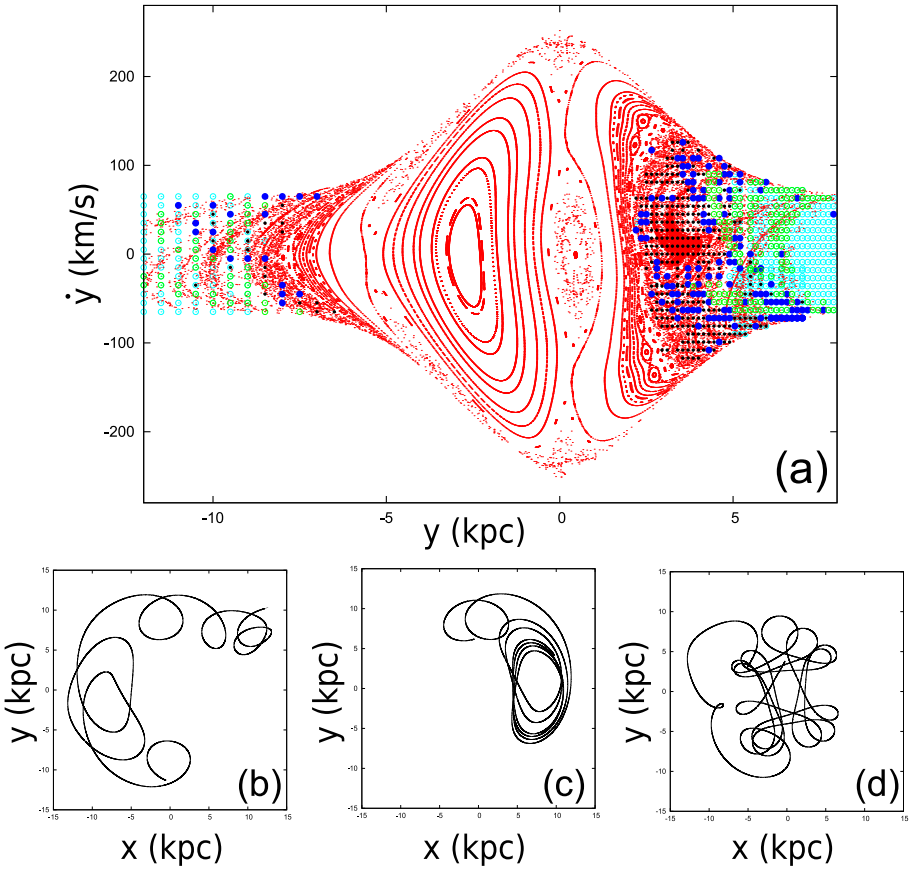

Figure 18. (a) Initial conditions of orbits on the $(y, \dot{y})$ surface of section for $E_J = -25650$ indicated according to their morphology within T_8. Open symbols correspond to orbits associated with banana-like morphologies like in (b) and (c). Filled symbols correspond to orbits having partly a 4:1 type morphology like the one in (d). The small black ones remain inside corotation, while the blue ones reinforce the outer spirals as well.

has enough particles at distances up to 4 times the bar radius. This allows us to study in detail the dynamical procedures taking place in these regions. We claim that the dynamics we present here bridge the orbital dynamics of barred and normal (non-barred) spiral galaxies.

The dynamical mechanisms we found acting in our model can be summarized as following:

- **Ordered elliptical flows.** Such flows shape the bar and the inner spirals (the strong spiral arms labelled with "A" in Fig. 2c).

The bar is formed by quasi-periodic orbits trapped around the stable x1 p.o. (aligned roughly along the major axis of the bar) as usual. However, in the central part of the bar, we have the formation of a boxy structure (Fig. 4) by orbits not related to the x1 family. This is discussed in detail elsewhere (paper II).

The ellipses of the x1 family precess beyond the region of the bar and support the inner spirals with quasi-periodic orbits that support an ordered, "precessing" flow (Fig. 8).

- **Chaotic orbits inside corotation.** In our model such orbits (Fig. 11), in a specific energy range, reinforce the extension of the spiral segments in region "2" (Fig. 6a). It is the second case encountered, where chaotic orbits inside corotation reinforce a structure (the other one has been presented by Patsis et al. (2010) and refers to the whole spiral structure of NGC 1300). Another role of these orbits, from a wider energy range, is the filling of the lemon-shaped disc area, which surrounds the inner barred-spiral structure.
- **The "hot orbital population".** This is by far the most important class of orbits for the overall morphology of the model. It shapes the outer spiral arms. It transfers particles from the inner disc area (where we have the inner spirals, "A", in Fig. 2c) to the outer disc area, beyond corotation, (where we have the outer spirals, "B", in Fig. 2c), through the L_1 and L_2 "gates". The amount of orbits returning to the inner disc region within T_8 is considerably smaller than these which stay outside corotation or practically escape.

As long as we consider chaotic orbits with $E_J > E_{(L_{1,2})}$ we consider orbits that in principle will explore all the available phase space if integrated for long enough time. However, at least for time T_8 we find that the outer spirals of the model are reinforced by chaotic orbits that clearly include two different characteristic imprints in their morphology. We call them "4:1-type" and "lpb-type" because they follow during a large fraction of T_8 a morphology resembling quasi-periodic orbits around 4:1-resonance-type orbits and around long-period-banana-like orbits respectively.

– *"4:1-type"*. This is the most common morphology of the orbits of the hot orbital population that support the outer spirals (Fig. 13b, Fig. 17d). This is expected, since such a morphology for chaotic orbits inside corotation already exist for $E_{(L_{1,2})} = -27772$ and keeps existing for all energies we found particles on orbits reinforcing the outer spirals. The lower the energy we find such chaotic orbits, the longer the time they spend on the average inside corotation, contributing to the surface density of the lemon-shaped inner disc region (inside corotation).

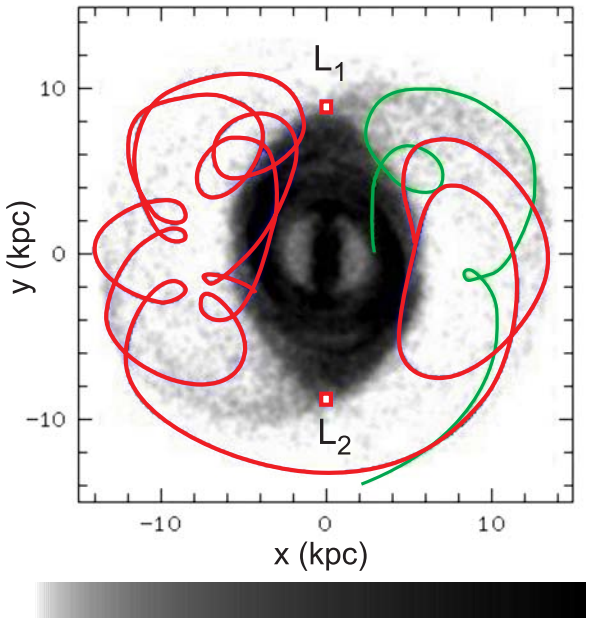

Figure 19. Two orbits with $E_J = -25650$ contributing to the surface density of the outer part of the spiral arms of our model, without visiting the immediate neighbourhood of L_1 or L_2 within T_8.

– *"lpb-type"*. We encounter this class of chaotic orbits for $E_J \gtrapprox -27000$, when the family of long period banana-like orbits is introduced in the system (Fig. 16b, Fig. 17b, Fig. 18b,c). The total amount of chaotic orbits, which support the outer spirals showing the lpb-type imprint in their morphology within T_8, is less than that of the 4:1-type, reflecting mainly the energy range in which we find each of them. However, with increasing energy, increases also the number of encountered hybrid morphologies (Fig. 16c, Fig. 17c, Fig. 18d). Finally such orbits contribute to the slight expansion of the inner, lemon-shaped, disc region to its sides (along the x-axis) and to the shaping of its outer border (Fig. 14).

A structure supported by quasi-periodic orbits, can be assigned to a family of stable p.o. with a specific morphology different in general from the morphology of the structure), that plays the role of its backbone. Intuitively, this cannot be done with a family of unstable p.o. and the chaotic orbits around them. Since we speak about chaotic orbits, we deal with orbits that share a common available phase space. In that sense it is unlikely to explain the reinforcement of a "chaotic" spiral structure (as the outer spiral arms in our model) by orbits along the asymptotic curve associated with the unstable orbits of a single family of p.o. (e.g. the PL1 and PL2 families). As correctly Tsoutsis et al. (2008) remark, it is a "coalescence of invariant manifolds" that leads to the formation of "chaotic" spirals. Nevertheless, statistics on the energies of the particles found in the arms and classification of the morphologies of their orbits point to two main classes of orbits, "4:1-type" and "lpb-type", which we mentioned above. Motivated from the morphology of the two prevailing patterns, we investigated the relation between the shape of the unstable periodic orbits that could be considered as a coarse shape of each of the two patterns (4:1-type and lpb-type) and the morphologies we find by integrating orbits along their unstable eigendirections. For energies close to $E_{(L_{1,2})}$ we find a close relation, because at these energies the vast majority of the particles that cross the L_1 and L_2 "gates" have a "4:1-type" past. The region where we find orbits supporting the chaotic spirals is occupied to a large extend by the unstable asymptotic curve of the 4:1-like unstable x1 p.o. (Fig. 15). For larger energies this relation becomes more vague, as we encounter a larger amount of orbits with hybrid morphologies in the area occupied by the asymptotic curve of the lpb p.o. (Fig. 17). At any rate the orbits we find primarily along the asymptotic curves of the x1 p.o. at the 4:1 resonance and $L_{1,2}$ energies, and secondarily the orbits along the asymptotic curves of the lpb p.o. at larger energies, give the morphologies of the orbits supporting the outer spirals of our model. Thus, they can be considered as the backbones of outer spiral arms structure.

We note that the largest part of the spiral arms extending beyond L_1 and L_2 (part "B" in Fig. 2) can be approximated by a logarithmic spiral about 20°. These arms are formed in a chaotic environment by means of an alternative mechanism of building spiral arms with pitch angles in this range, besides the one proposed by Pérez-Villegas et al. (2012) in models for normal spirals.

Practically, the "4:1-type" orbits are orbits of the same kind that form also the "chaotic" spirals in the case of the NGC 4314 model in Patsis (2006), which in turn are the same chaotic orbits building the envelope of the bar in the same potential in Patsis et al. (1997). In the present case the envelope of the bar of the NGC 4314 model corresponds to the lemon-shaped disc region, which surrounds the barred-spiral structure. This is a consequence of the $R_c/R_b = 2.9$ ratio we have in the model. Pushing the $L_{1,2}$ points away from the ends of the bar we allow the coexistence of two different dynamical mechanisms acting in the same model and support two pairs of spiral arms. Such double spirals exist in some cases of grand design galaxies with morphologies that resemble that of our model. Two examples are NGC 1566 and NGC 5248. Their DSS images are given in Fig. 20. Despite the fact that our model does not refer explicitly to these galaxies and although optical images are a combination of many physical parameters (dust attenuation, population effects etc., see Zibetti et al. (2009)) the observed overall morphology is to some degree indicative of the underlying dynamics. The images have not been corrected for projection effects, however they are face-on enough so that we can identify the features we discuss. We have used appropriate look-up-tables and values for the contrast of the images and we have flipped the images so that the spirals have similar orientation with the models in Fig. 2 , in order to facilitate the comparison. The outer spirals are very weak features in NIR images of these galaxies (for NGC 1566 see Grosbøl & Dottori (2012)) indicating that they are consisting mainly of young objects and gas. This is in agreement with our finding that "chaotic" spirals are features enhanced in gaseous models (Tsigaridi & Patsis 2010; Patsis 2012). There is a conspicuous correspondence between the morphological characteristics of these two galaxies and the features developed in our models (Fig. 2). The two sets of spirals, inner and outer, are labelled again with "A" and "B" as in Fig. 2. The lemon-shaped inner disc region is emphasized in Fig. 20a by the outermost of the drawn isophotes, while in Fig. 20b it extends inside the dark envelope around a white region surrounding the inner barred-spiral pattern. According to our models, the approximate location of L_1 and L_2 in the systems depicted in the images of the galaxies would be close to the drawn white filled circles, just at the beginning of the outer spiral arms. In conclusion, the two galaxies reproduce in an archetypical way the double mechanism that leads to the inner spiral structure supported by regular orbits (as in the case of normal spirals) and the outer "chaotic" spirals (as in the case of

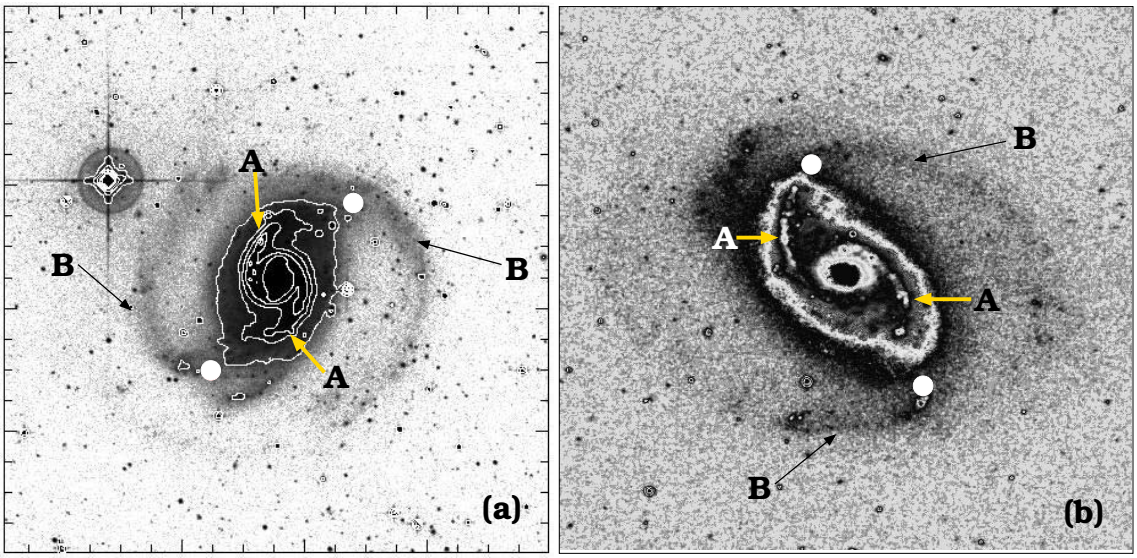

Figure 20. Optical (red) DSS images of (a) NGC 1566 and (b) NGC 5248. The correspondence of their morphologies with the structure of our model (Fig. 2) is apparent.

barred-spirals). In that respect they can be considered as bridging the dynamics of the two types of spiral galaxies.

Different kinds of barred-spiral response morphologies are developed in models with different pattern speeds as the result of the action of only some of these mechanisms. These models, and special dynamical features characterizing them, are presented in subsequent papers.

Acknowledgements

We thank Prof. G. Contopoulos for fruitful discussions. This work has been partially supported by the Research Committee of the Academy of Athens through the project 200/795. We acknowledge the use of data from The Digitized Sky Survey produced at the Space Telescope Science Institute under U.S. Government grant NAG W-2166. The images of these surveys are based on photographic data obtained using the Oschin Schmidt Telescope on Palomar Mountain and the UK Schmidt Telescope. The plates were processed into the present compressed digital form with the permission of these institutions.

REFERENCES

Athanassoula E, 2012, MNRAS 426L, 46
Athanassoula E, Misiriotis A., 2002, MNRAS 330, 35
Athanassoula E., Romero-Gomez M., Bosma A., Masdemont J. J., 2010, MNRAS 407, 1433
Chatzopoulos S., Patsis P. A., Boily C.M., 2011, MNRAS 416, 479
Contopoulos G., 1970, AJ 75, 96
Contopoulos G., 2009, in *Chaos in Astronomy*, Contopoulos G., Patsis P.A. (eds.), Springer Verlag, Heidelberg. pp 3-22
Contopoulos G. & Grosbøl P., 1986, A&A 155, 11
Contopoulos G. & Grosbøl P., 1988, A&A 197, 83
Contopoulos G. & Grosbøl P., 1989, A&ARv, 1, 261
Contopoulos G. & Polymilis C., 1993, Phys. Rev. E 47, 1546
Efthymiopoulos C., 2010, Eur. Phys. J. S.T., 186, 91
Grosbøl P., Dottori H., 2012, A&A, 542A, 39
Harsoula M., Kalapotharakos C., 2009, MNRAS 394, 1605
Harsoula M., Kalapotharakos C., Contopoulos G., 2011, MNRAS 411, 1111
Hénon M., 1965, AnAp, 28, 499
Kalapotharakos C., Patsis P.A., Grosbøl P. 2010a, MNRAS 403, 83
Kaufmann D.E., Contopoulos G., 1996, A&A, 309, 381
Lépine J. R. D., Roman-Lopes A., Abraham, Z. et al., 2011, MNRAS 414, 1607
Martos M., Hernanadez X., Yanez M. et al., 2004, MNRAS 350L, 47
Patsis P.A., 2005, MNRAS 358, 305
Patsis P.A., 2006, MNRAS 369L, 56
Patsis P.A., 2009, in *Chaos in Astronomy*, Contopoulos G., Patsis P.A. (eds.), Springer Verlag, Heidelberg. pp 33-44
Patsis P.A., 2012, Int. J. Bif. Ch. 22, No9, 1230029
Patsis P. A., Contopoulos G., Grosbøl P., 1991, A&A, 243, 373
Patsis P. A., Athanassoula E., Quillen A. C., 1997, ApJ, 483, 731
Patsis P. A., Kalapotharakos C., 2011, Mem. S.A. It. S., 18, 83
Patsis P. A., Kaufmann, D. E., Gottesman S.T., Boonyasait, V., 2009, MNRAS 394, 142
Patsis P. A., Kalapotharakos C., Grosbøl P., 2010, MNRAS 408, 22
Patsis P.A., Tsigaridi L., 2013, in preparation (Paper III)
Pérez-Villegas A., Pichardo B., Moreno E., Peimbert A., Velásquez H.M., 2012, ApJL 745, L14
Pfenniger D., Friedli D., A&A 252, 75
Romero-Gómez M., Masdemont J. J., Athanassoula E., García-Gómez C. 2006, A&A 453, 39
Tsigaridi L., Patsis P.A., 2010, in *"Advances in Hellenic Astronomy during the IYA09"*, ASP Conf. Ser. Vol. 424, K. Tsinganos, D. Hadzidimitriou, T. Matsakos (eds), pp.382-383
Saha K., Naab Th., 2013, arXiv:1304.1667
Tsigaridi L., Patsis P.A., 2013b, in preparation (Paper II)
Tsoutsis P., Efthymiopoulos C., Voglis N., 2008, MNRAS 387, 1264
Tsoutsis P., Kalapotharakos C., Efthymiopoulos C., Contopoulos G., 2009, A&A 495, 743

de Vaucouleurs G., de Vaucouleurs A., Corwin H. G. Jr, et al. 1991,"Third Reference Catalogue of Bright Galaxies" (RC3), Springer, NY
Voglis N., Stavropoulos I., 2005, in "*Recent advances in Astronomy and Astrophysics*", N. Solomos (ed), AIP Conference Proceedings, Volume 848, pp. 647-659
Voglis N., Stavropoulos I., Kalapotharakos C., 2006, MNRAS 372, 901
Zhang X., Buta R., 2007, AJ 133, 2584
Zibbeti S., Charlot S., Rix H-W. 2009, MNRAS 400, 1181